AGU PUBLICATIONS

JGR

Journal of Geophysical Research: Space Physics

RESEARCH ARTICLE
10.1002/2013JA019310

Key Points:
- Radiation belt pitch angle scattering within the drainage plume is strong
- The amount of scattering agrees with diffusion coefficients in the literature
- The pitch angle scattering leads to radial transport of the radiation belt

Correspondence to:
J. E. Borovsky,
jborovsky@spacescience.org

Citation:
Borovsky, J. E., R. H. W. Friedel, and M. H. Denton (2014), Statistically measuring the amount of pitch angle scattering that energetic electrons undergo as they drift across the plasmaspheric drainage plume at geosynchronous orbit, *J. Geophys. Res. Space Physics*, *119*, 1814–1826, doi:10.1002/2013JA019310.

Received 9 AUG 2013
Accepted 16 FEB 2014
Accepted article online 22 FEB 2014
Published online 19 MAR 2014

Statistically measuring the amount of pitch angle scattering that energetic electrons undergo as they drift across the plasmaspheric drainage plume at geosynchronous orbit

Joseph E. Borovsky[1,2,3], Reiner H. W. Friedel[4], and Michael H. Denton[2,3]

[1]AOSS, University of Michigan, Ann Arbor, Michigan, USA, [2]Center for Space Plasma Physics, Space Science Institute, Boulder, Colorado, USA, [3]Department of Physics, Lancaster University, Lancaster, UK, [4]Los Alamos National Laboratory, Los Alamos, New Mexico, USA

Abstract Using five spacecraft in geosynchronous orbit, plasmaspheric drainage plumes are located in the dayside magnetosphere and the measured pitch angle anisotropies of radiation belt electrons are compared duskward and dawnward of the plumes. Two hundred twenty-six plume crossings are analyzed. It is found that the radiation belt anisotropy is systematically greater dawnward of plumes (before the electrons cross the plumes) than it is duskward of plumes (after the electrons have crossed the plumes). This change in anisotropy is attributed to pitch angle scattering of the radiation belt electrons during their passage through the plumes. A test database in the absence of plumes finds no equivalent change in the radiation belt anisotropy. The amount of pitch angle scattering by the plume is quantified, scattering times are estimated, and effective pitch angle diffusion coefficients within the plume are estimated. The pitch angle diffusion coefficients obtained from the scattering measurements are of the same magnitude as expected values for electromagnetic ion cyclotron (EMIC) waves at high electron energies (1.5 MeV); however, expected EMIC diffusion coefficients do not extend to pitch angles of 90° and would have difficulties explaining the observed isotropization of electrons. The pitch angle diffusion coefficients obtained from the scattering measurements are of the same magnitude as expected values for whistler mode hiss at lower electron energies (150 keV). Outward radial transport of the radiation belt caused by the pitch angle scattering in the plume is discussed.

1. Introduction

As the electrons of the outer electron radiation belt circulate around the Earth, they undergo interaction with the plasma waves of the magnetosphere. One important result of these wave-particle interactions is pitch angle scattering [*Lyons and Thorne*, 1973; *Shprits et al*., 2009; *Artemyev et al*., 2012]. This scattering is thought to be particularly strong as the radiation belt electrons drift across the plasmaspheric drainage plume that sometimes resides in the dayside magnetosphere [*Spasojevic et al*., 2004; *Fraser et al*., 2006; *Bortnik et al*., 2006; *Yahnin and Yahnina*, 2007; *Millan and Thorne*, 2007; *Jordanova et al*., 2007]. The high-density lumpy drainage plume is anticipated to be the site of electromagnetic ion cyclotron (EMIC) waves [e.g., *Kovalevskiy*, 1980, 1981; *Jordanova et al*., 2006; *Thorne et al*., 2006; *Spasojevic and Fuselier*, 2009] and plasmaspheric hiss [e.g., *Chan and Holzer*, 1976; *Hayakawa et al*., 1986; *Summers et al*., 2008].

Anisotropies of the pitch angle distributions of the radiation belt electrons are driven largely by drift shell splitting in the presence of a radially inward flux gradient [*Hones*, 1963; *Pfitzer et al*., 1969; *Selesnick and Blake*, 2002] as the electrons orbit the Earth in a field that is weakened from dipole values by plasma diamagnetism on the nightside [*Borovsky and Denton*, 2010a] and strengthened above dipole values by the Chapman-Ferraro current on the dayside. (Note that this nightside-dayside pattern can be reversed during geomagnetic storms at low solar wind Mach numbers [cf. *Borovsky et al*., 2009, 2013].) In the dayside magnetosphere the outer electron radiation belt pitch angle distribution is usually dominated by fluxes of electrons perpendicular to B (pitch angles $\alpha \sim 90°$) with weak fluxes parallel to B [cf. *West et al*., 1973; *Gannon et al*., 2007; *Borovsky and Denton*, 2011]; the opposite trend (parallel dominance) is seen on the nightside [cf. *Borovsky and Denton*, 2011].

A sketch of the equatorial plane of the magnetosphere appears in Figure 1. The plasmaspheric drainage plume, composed of cold plasma flowing sunward from low *L* shells to the dayside reconnection X line on the

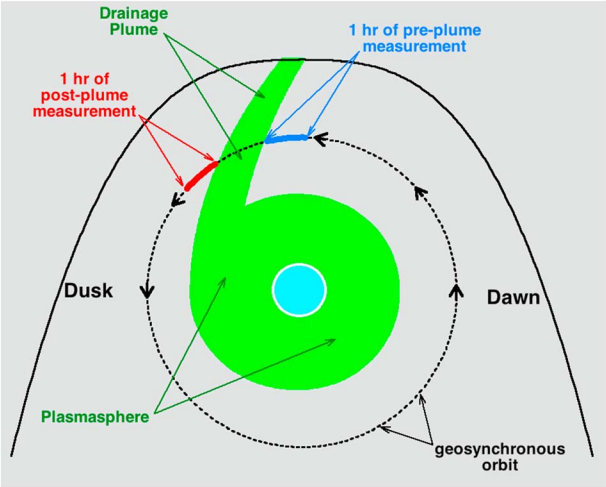

Figure 1. A sketch of the equatorial plane of the magnetosphere showing how geosynchronous orbit (black dashed curve) cuts through the plasmaspheric drainage plume (green) in the dayside magnetosphere. The direction of motion of spacecraft in geosynchronous orbit is shown with the black arrowheads. (This is also the direction of the radiation belt electron drift.) Each time a spacecraft crosses a plume, 1 h of measurements is extracted before entering the plume (blue) and 1 h of measurements is extracted after exiting the plume (red).

magnetopause, is shown in green. Geosynchronous orbit ($L = 6.6$) is shown as the black dashed circle. As spacecraft in geosynchronous orbit pass through the dayside magnetosphere from dawn to noon to dusk, they pass through the plasmaspheric drainage plume [*Denton and Borovsky*, 2008; *Borovsky and Denton*, 2008]. Drainage plumes are a persistent feature of geomagnetic storms: experience with the magnetospheric plasma analyzer (MPA) [*Bame et al.*, 1993; *Thomsen et al.*, 1999] data set at geosynchronous orbit has taught the authors that as long as the *Kp* index is elevated, the MPA spacecraft will consistently detect a plume in the dayside magnetosphere.

The amount of pitch angle scattering that radiation belt electrons undergo as they cross through the plume plasma in their drift orbits will be statistically measured by comparing radiation belt anisotropy measurements just dawnward of the plumes (before the electrons cross) with radiation belt anisotropy measurements just duskward of the plumes (after the electrons cross). Plumes will be located using the MPA instruments on five spacecraft in geosynchronous orbit, and the radiation belt anisotropies will be measured by the synchronous orbit particle analyzer (SOPA) instruments [*Belian et al.*, 1992; *Cayton and Belian*, 2007] on the same five spacecraft. To build statistics, 226 plume crossings will be analyzed.

This manuscript is organized as follows. In section 2 the methodology of the measurements is described, and the results of the measurements are shown in section 3. A test of the scattering-measurement technique in the absence of drainage plumes is described in section 4. In section 5 scattering times are calculated for one at geosynchronous orbit associated with the drainage plume. In section 6 the pitch angle diffusion coefficient within the plume at geosynchronous orbit is estimated from the scattering measurements. In section 7 the radial transport and radial diffusion of the electron radiation belt associated with the pitch angle scattering is estimated. Section 8 contains discussions about the local time pattern of radiation belt anisotropy and about consequences of the pitch angle scattering.

2. Measuring the Pitch Angle Scattering

The amount of pitch angle scattering that radiation belt electrons undergo as they make a single crossing of the plasmaspheric drainage plume in the dayside magnetosphere will be measured by statistically comparing the measured anisotropy of the electrons before they cross the plume with their measured anisotropy after they cross the plume.

The before and after measurements of the radiation belt anisotropy will be attained from 226 crossings of drainage plumes by five geosynchronous orbit spacecraft carrying the SOPA energetic-particle instruments. The anisotropy will be measured in two energy bands: 1.3–1.7 MeV and 120–180 keV. This two-energy band anisotropy data set was assembled for the radiation belt anisotropy survey of *Borovsky and Denton* [2011]. Ten minute averages of the measured fluxes will be used from satellites that spin with ~10 s periods. Each SOPA instrument contains three electron telescopes mounted on a satellite with an Earth-pointing spin axis [*Cayton and Belian*, 2007]. Without a magnetometer on board the spacecraft, the magnetic field direction at the satellite is determined from the anisotropy axis of the electron flux measurements, and that magnetic field direction is used to sort the electron flux measurements into pitch angle. The pitch angle distributions are assumed to be symmetric, about 90°, so the pitch angle measurements are reflected about 90°. For the

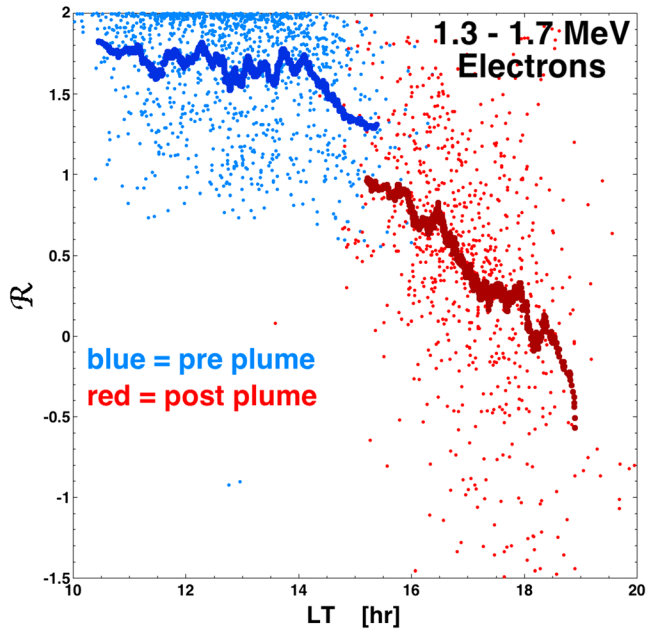

Figure 2. From 226 plume crossings, 1 h of 10 min averages of the anisotropy ratio so 1.3–1.7 MeV electrons are extracted dawnward of each plume and plotted as the blue points and 1 h of 10 min averages of the anisotropy ratio is extracted duskward of each plume and plotted as the red points. A 50-point running average of the blue plotted points is plotted in dark blue and, a 50-point running average of the red plotted points is plotted in dark red.

Borovsky and Denton [2011] survey the ratio A of the average flux F in the field-aligned directions (15°–45°) to the average flux F in the perpendicular directions (45°–90°) was used, written

$$A = \langle F(15° - 45°)\rangle / \langle F(45° - 90°)\rangle. \quad (1)$$

Pitch angles between 0° and 15° are not used in this parameter A owing to the poorer coverage by SOPA of this region of phase space. This measure is converted into the anisotropy ratio R defined as

$$R = \left(F_{\perp} - F_{||}\right)/\left(0.5\left(F_{\perp} + F_{||}\right)\right) = 2(1 - A)/(1 + A). \quad (2)$$

The ratio R ranges in value from $R = -2$ (parallel dominated) to $R = 0$ (isotropic) to $R = +2$ (perpendicular dominated).

Plasmaspheric drainage plumes are located using the MPA measurements on the same five spacecraft that carry the SOPA instruments. The drainage plumes are identified as regions of dense (n greater than ~10 cm^{-3}) cool ($T \sim 1$ eV) plasma that resides within a spatial gap in the electron plasma sheet [cf. *Borovsky et al.*, 2013, Figures 13 and 19]. The warm plasma cloak ($n \sim 5$ cm^{-3}, $T \sim 10$ eV, and oxygen rich) [cf. *Chappell et al.*, 2008; *Borovsky et al.*, 2013] residing within the electron plasma sheet in the dayside magnetosphere is not included as part of the drainage plume. Using MPA, the times at which the spacecraft enter into and exit from the plumes are noted and 1 h of SOPA anisotropy measurements is collected immediately prior to plume entry (dawnward of the plume) and 1 h of SOPA anisotropy measurements is collected immediately after plume exit (duskward of the plume). These anisotropy collection intervals are indicated in blue and in red along geosynchronous orbit in Figure 1.

The 226 plume crossings occurred during multiple-daylong high-speed stream-driven storms in the years 2003–2005. The storms are from a collection of high-speed stream-driven storms used in prior studies of the magnetosphere and radiation belt [e.g., *Borovsky and Denton*, 2010b; *Denton and Borovsky*, 2012]; the set of storms used overlaps with available radiation belt anisotropy measurements. High-speed stream-driven storms have well-developed plasmaspheric drainage plumes (and the evolution of the outer electron radiation belt is of particular interest during these high-speed stream-driven storms) [*Paulikas and Blake*, 1976; *Friedel et al.*, 2002; *Borovsky and Denton*, 2006, 2010b; *McPherron et al.*, 2009; *Lam et al.*, 2009]. Plumes shift in local time and change in intensity but are persistently seen as one MPA spacecraft after another cross through the dayside magnetosphere [*Borovsky and Denton*, 2008]. It is very rare that an MPA spacecraft does not see the plume during a crossing of the dayside magnetosphere during a storm.

3. Results of the Measurements

In Figure 2, 10 min averaged values of the SOPA-measured anisotropy ratio R are plotted as a function of local time for the energy channel 1.3–1.7 MeV. Anisotropy measurements taken within 1 h of local time before electrons enter into the plume are plotted in blue, and measurements taken within 1 h of local time after electrons exit the plume are plotted in red. Note that for each of the 226 plumes, the local time positions of the two edges of the plume vary: the plume varies in width and the plume varies in local time position [cf. *Borovsky and Denton*, 2008; *Borovsky et al.*, 2013].

Table 1. Estimating the Pitch Angle Scattering Times for Radiation Belt Electrons From the Measured Anisotropy Values Across the Plasmaspheric Drainage Plume at Geosynchronous Orbit

	1.3–1.7 MeV	120–180 keV
R_{pre}	1.30	0.38
R_{post}	0.98	0.17
$\Delta R = R_{pre} - R_{post}$	0.32	0.21
$\Delta R/R_{pre}$	0.246	0.553
$\Delta t = \tau_{drift}$	440 s	3100 s
$\Delta R/\Delta t$	7.27×10^{-4} s^{-1}	6.77×10^{-5} s^{-1}
$\tau_{isot} = R_{pre}/(\Delta R/\Delta t)$	1800 s = 30 m	5600 s = 93 m
$N = \tau_{isot}/\tau_{drift}$	4.1	1.8

Plotted in dark blue in Figure 2 is a 50-point running average of the points in blue, and plotted in dark red is a 50-point running average of the points in red. The running averages reduce the vertical spread in the data points and reveal the underlying statistical trend. As can be seen, there is a vertical gap between the dark -blue and the dark red running averages. This vertical gap is consistent with the electrons undergoing pitch angle scattering toward isotropy within the plume: the electrons are statistically more isotropic after plume passage (red) than before the passage (blue). If there were no scattering, then the two running-average curves should approximately meet. (This meeting in the absence of plumes will be tested in section 4.) In the gap region where the R values of the two populations can be seen clearly, the average value of R before entering the plume is $R_{pre} = 1.30$ (dark blue curve) and the average value of R after crossing the plume is $R_{post} = 0.98$ (dark red curve). These values are entered into Table 1.

For the 1.3–1.7 MeV electrons with an anisotropy ratio $R_{pre} = 1.30$ before plume crossing and an anisotropy ratio $R_{post} = 0.98$ after plume crossing, the fractional reduction in the anisotropy ratio $\Delta R/R = (R_{pre} - R_{post})/R_{pre}$ after one plume crossing is 0.246 (cf. Table 1): this is equivalent to a reduction of the anisotropy ratio of these 1.3–1.7 MeV electrons by 25% during a single plume crossing by the electrons.

In Figure 3, 10 min averaged values of the SOPA-measured anisotropy ratio R are plotted as functions of local time for the energy channel 120–180 keV. Anisotropy measurements taken within 1 h of local time before electrons enter into the plume are plotted in blue and measurements taken within 1 h of local time after electrons exit the plume are plotted in red.

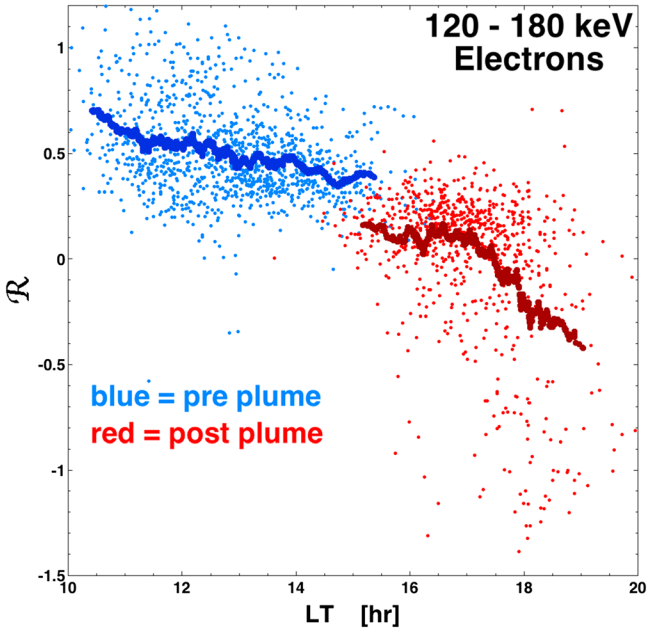

Figure 3. From 226 plume crossings, 1 h of 10 min averages of the anisotropy ratio so 120–180 keV electrons are extracted dawnward of each plume and plotted as the blue points and 1 h of 10 min averages of the anisotropy ratio is extracted duskward of each plume and plotted as the red points. A 50-point running average of the blue plotted points is plotted in dark blue, and a 50-point running average of the red plotted points is plotted in dark red.

Plotted in dark blue in Figure 3 is a 50-point running average of the points in blue, and plotted in dark red is a 50-point running average of the points in red. As was the case for the 1.3–1.7 MeV energy channel of Figure 2, there is a vertical gap between the dark blue and dark red running averages in Figure 3. This vertical gap is consistent with the 120–180 keV electrons undergoing pitch angle scattering toward isotropy within the plume: the electrons are statistically more isotropic after they exit the plume (red) than before they enter the plume (blue). In the gap region where the R values of the two populations can be seen clearly, the average value of R before entering the plume is $R_{pre} = 0.38$ (dark blue curve) and the average value of R after crossing the plume is $R_{post} = 0.17$ (dark red curve). The values are entered into Table 1.

For the 120–180 keV electrons with an anisotropy ratio $R_{pre} = 0.38$ before plume crossing and an anisotropy ratio $R_{post} = 0.17$ after plume crossing, the

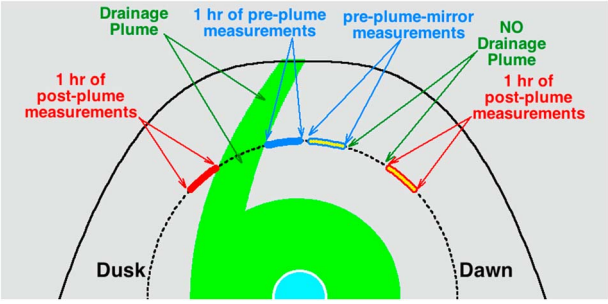

Figure 4. A sketch of the equatorial plane of the magnetosphere showing the locations where preplume and postplume measurements are taken and showing the locations of the no-plume data intervals mirrored across local noon.

fractional reduction in the anisotropy ratio $\Delta R/R = (R_{pre} - R_{post})/R_{pre}$ after one plume crossing is 0.553 (cf. Table 1): this is equivalent to a reduction of the anisotropy ratio by 55% during a single plume crossing of the 120–160 keV electrons.

4. A No-Plume Test in the Morning Sector

In section 3 it was stated that the vertical gaps between the preplume anisotropies and the postplume anisotropies in Figures 2 and 3 are consistent with pitch angle scattering of electrons within the plasmaspheric drainage plume. As a test of this explanation for the gap, one would like to examine anisotropy measurements in the afternoon magnetosphere in the absence of a plume. However, during geomagnetic storms when the *Kp* index is elevated, there is essentially always a drainage plume in the afternoon sector, so a data set in this region in the absence of a plume cannot be obtained.

However, in the morning sector there is almost never a drainage plume. Here a test of the association of the gap with the action of the plume can be performed. To do this no-plume test, "mirror" data sets to the afternoon preplume anisotropies and postplume anisotropies are obtained as follows. For each spacecraft traversal across the dayside magnetosphere in which anisotropy data are collected around a plume, data from the local times mirrored across local noon are also collected. For example, if a preplume hour of data is taken from 13 to 14 LT, then an interval of preplume-mirrored data is taken from 11 to 10 LT. And likewise, if a postplume interval of data is collected at 16.5–17.5 LT, then a postplume-mirrored interval of data is collected at 7.5–6.5 LT. This mirroring of the preplume and postplume data collection is sketched in Figure 4. The original data intervals straddling the plume are sketched in blue (pre) and red (post); the mirrored data intervals are sketched in blue and yellow (premirrored) and red and yellow (postmirrored). The mirrored pre-data sets and post data sets, focused around the absence of a plume in the morning sector of the magnetosphere, will be analyzed as are the original pre-data sets and post data sets focused around the presence of a plume in the afternoon sector of the magnetosphere.

In Figure 5 (right) the 50-point running average of the preplume 1.3–1.7 MeV anisotropy ratios is plotted in blue, and the 50-point running average of the post plume 1.3–1.7 MeV anisotropy ratios are plotted in red (cf. Figure 2). The vertical gap between the two curves is clearly seen. In Figure 5 (left) the 50-point running average of the preplume-mirrored 1.3–1.7 MeV anisotropy ratios are plotted in blue, and the 50-point running average of the postplume-mirrored 1.3–1.7 MeV anisotropy ratios are plotted in red. Note that there is no vertical gap between the two curves in the Figure 5 (left). In the absence of a plume (in particular in the absence of pitch angle scattering within a plume) there is no offset in the anisotropy ratios of the two curves. Hence, it is consistent that the vertical gap between the two curves in the Figure 5 (right) (and in Figure 2) is owed to pitch angle scattering of 1.3–1.7 MeV radiation belt electrons as they drift through the plasmaspheric drainage plume.

In Figure 6 (right) the 50-point running average of the preplume 120–180 keV anisotropy ratios is plotted in blue, and the 50-point running average of the postplume 120–180 keV anisotropy ratios are plotted in red (cf. Figure 3). The vertical gap between the two curves is clearly seen. In Figure 6 (left) the 50-point running average of the preplume-mirrored anisotropy ratios are plotted in blue, and the 50-point running average of the postplume-mirrored anisotropy ratios are plotted in red. As was the case in Figure 5, there is no vertical gap between the two curves in Figure 6 (left). In the absence of pitch angle scattering within a plume there is no offset in the anisotropy ratios of the two curves. Hence, it is consistent that the vertical gap between the two curves in Figure 6 (right) (and in Figure 3) is owed to pitch angle scattering of 120–180 keV radiation belt electrons as they drift through the plasmaspheric drainage plume.

A second indication of the lack of scattering in the absence of plumes will come in section 8 where the diurnal pattern of radiation belt anisotropy across the dayside magnetosphere is examined at low *Kp* (where plumes are rare) versus at high *Kp* (where plumes are prevalent).

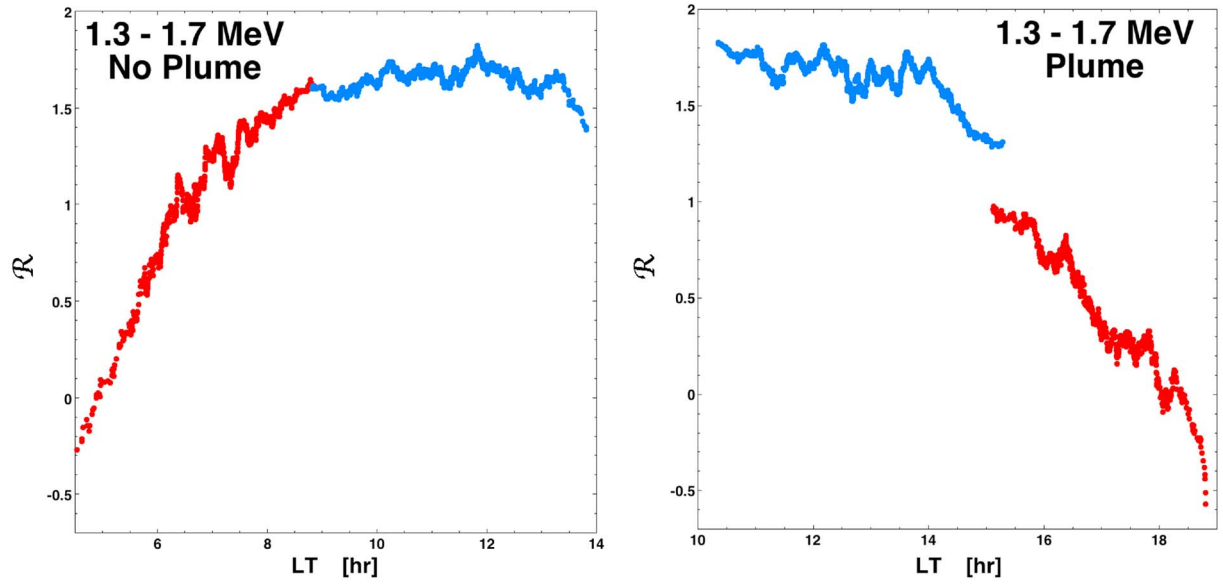

Figure 5. For the 226 plume crossings, (right) 50-point running averages of the preanisotropy (blue) and postanisotropy (red) 1.3–1.7 MeV ratios are plotted versus local time and (left) 50-point running averages of the premirrored (blue) and postmirrored (red) 1.3–1.7 MeV anisotropy ratios are plotted versus local time. The data sets in Figure 5 (right) straddle the drainage plume whereas the data sets in Figure 5 (left) straddle a region without a plume.

5. Scattering Times

At the end of section 3 the change $\Delta R = R_{pre} - R_{post}$ in the anisotropy ratio R that electrons undergo in a single drift through the dayside plasmaspheric drainage plume was measured (cf. Table 1) and the fractional reduction of their anisotropy $\Delta R/R_{pre}$ for that single passage through the plume was calculated. For 1.3–1.7 MeV electrons the reduction in the anisotropy ratio for a single crossing of the plume is $\Delta R/R_{pre} = 25\%$ (cf. Table 1), and for 120–180 keV electrons the reduction in the anisotropy ratio for a single crossing of the plume is $\Delta R/R_{pre} = 55\%$.

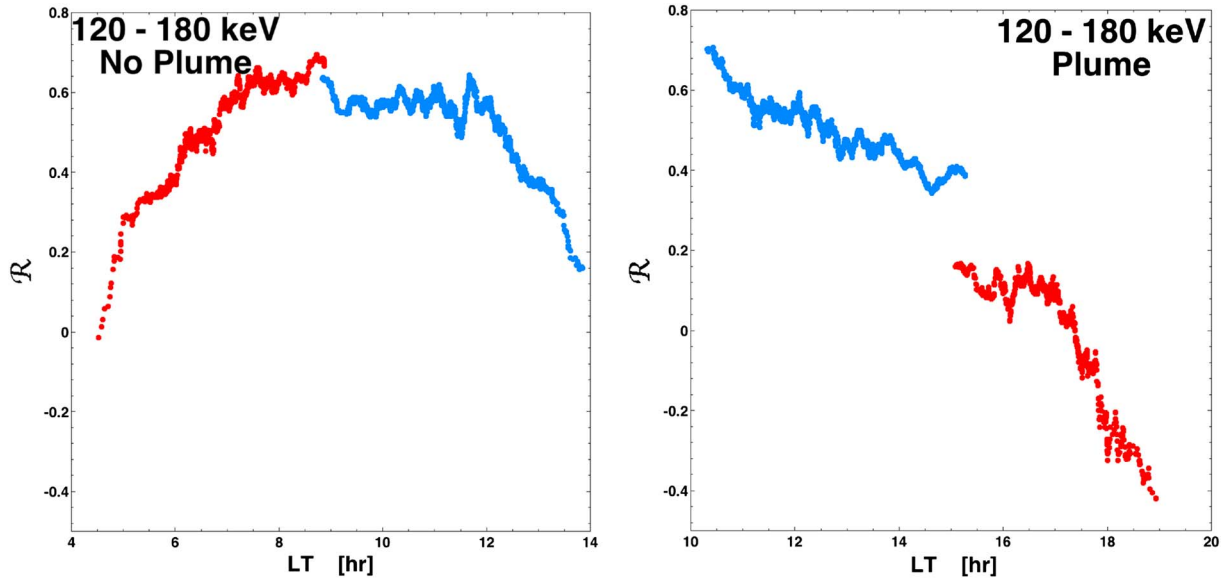

Figure 6. For the 226 plume crossings, (right) 50-point running averages of the preanisotropy (blue) and postanisotropy (red) 120–180 keV ratios are plotted versus local time and (left) 50-point running averages of the premirrored (blue) and postmirrored (red) 120–180 keV anisotropy ratios are plotted versus local time. The data sets in the Figure 6 (right) straddle the drainage plume whereas the data sets in Figure 6 (left) straddle a region without a plume.

Table 2. Estimating the Pitch Angle Diffusion Coefficient $D_{\alpha\alpha}$ Inside of the Drainage Plume at Geosynchronous Orbit

	1.3–1.7 MeV	120–180 keV
$N = \tau_{isot}/\tau_{drift}$	4.1	1.8
τ_{drift}	440 s	3100 s
$\tau_{cross} = (5/24)\tau_{drift}$	92 s	645 s
$\tau'_{isot} = N\,\tau_{drift}$	375 s	1160 s
$D_{\alpha\alpha} = (\Delta\alpha)^2/\tau'_{isot}$	7.3×10^{-4} rad^2 s^{-1}	2.4×10^{-4} rad^2 s^{-1}

From these measurements, a pitch angle scattering time owing to the plasmaspheric drainage plume is estimated as follows. The scattering time τ_{isot} can be expressed as

$$\tau_{isot} = R/(dR/dt) = R_{pre}/(\Delta R/\Delta t) \quad (3)$$

where ΔR is the change in R for a single crossing of the plume ($\Delta R = R_{pre} - R_{post}$) and Δt is the interval between electron crossings of the plume. The Δt is the around-the-Earth drift period of the electrons τ_{drift}. The drift period at geosynchronous orbit can be approximated as

$$\tau_{drift} = \tau_o(1 + E)/(E(2 + E)) \quad (4)$$

[*Chanteur et al.*, 1978] where $\tau_o \sim 1600$ s and $E = E/m_ec^2$ where E is the kinetic energy of the drifting electron. For $E = 1.5$ MeV expression (4) yields $\tau_{drift} = 440$ s, and for $E = 150$ keV expression (4) yields $\tau_{drift} = 3100$ s: these values are entered into Table 1. Using these values of τ_{drift} for Δt in expression (3) and using the values of R_{pre} and ΔR from Table 1, the scattering time is estimated to be $\tau_{isot} = 1800$ s for 1.3–1.7 MeV electrons and the scattering time is estimated to be $\tau_{isot} = 5600$ s for 120–180 keV electrons.

The ratio of the scattering time τ_{isot} to the drift period τ_{drift} indicates the number $N = \tau_{isot}/\tau_{drift}$ of plume crossings required for electron anisotropy to be reduced by a multiplicative factor of $1/e$. For 1.3–1.7 MeV electrons the number of plume crossings is $N = 4.1$ and for 120–180 keV electrons the number of plume crossings is $N = 1.8 \sim 2$. These values are entered into Table 1.

6. The Pitch Angle Diffusion Coefficients Within the Plume

The order of magnitude of the pitch angle diffusion coefficient $D_{\alpha\alpha}$ within the plume that results in the observed amount of scattering can be estimated as follows. In Table 1 the number of plume crossings N required to isotropize the electrons is given: that number is copied into Table 2. A typical drainage plume is about 5 h wide in local time at geosynchronous orbit [*Borovsky and Denton*, 2008; *Borovsky et al.*, 2013]. Hence, a plume crossing time τ_{cross} is about 5/24 of an around-the-Earth drift period τ_{drift}, written $\tau_{cross} = 5\tau_{drift}/24$. Using the τ_{drift} values in Table 1, for 1.5 MeV electrons this is $\tau_{cross} \sim 92$ s and for 150 keV electrons this is $\tau_{cross} \sim 645$ s. The scattering time τ'_{isot} that would result if the electrons were to travel only in plume plasma is (by the definition of N in section 5) $\tau'_{isot} = N\tau_{cross}$. Hence, $\tau'_{isot} \sim 375$ s for 1.5 MeV electrons and $\tau'_{isot} \sim 1160$ s for 150 keV electrons. Examining the pitch angle diffusion equation $\partial f/\partial t = D_{\alpha\alpha}\,\partial^2 f/\partial\alpha^2$, for full isotropization

$$D_{\alpha\alpha} = (\Delta\alpha)^2/\tau'_{isot}. \quad (5)$$

Scattering here is measured between the fluxes in a band at $\alpha = 15°$–$45°$ and the fluxes in a band at $\alpha = 45°$–$90°$ (cf. section 2): looking at mirror symmetry about 90° these two pitch angle bands are separated by 60°, so the gradient scale is $\Delta\alpha = 30°$ for a second derivative. For 1.3–1.7 MeV electrons expression (5) with $\Delta\alpha = 30°$ and $\tau'_{isot} \sim 375$ s yields $D_{\alpha\alpha} \sim 2.4$ deg^{2}s$^{-1} = 7.3 \times 10^{-4}$ rad^{2}s^{-1}. For 120–180 keV electrons expression (5) with $\Delta\alpha = 30°$ and $\tau'_{isot} \sim 1160$ s yields $D_{\alpha\alpha} \sim 0.78$ deg^{2}s$^{-1} = 2.4 \times 10^{-4}$ rad^{2}s^{-1}. These values are entered into Table 2. Note that $D_{\alpha\alpha}$ could easily vary by a factor of 2 or more since the plume width varies by a factor of 2 [cf. *Borovsky et al.*, 2013, Figure 16].

The $D_{\alpha\alpha}$ value of 2.4 deg^{2}s^{-1} obtained for 1.5 MeV electrons is of the same magnitude as the theoretical 1.5 MeV EMIC wave values for $D_{\alpha\alpha}$ near geosynchronous orbit (with $n_e = 55$ cm^{-3}) plotted in *Jordanova et al.* [2008, Figure 2]. However, theoretical EMIC pitch angle diffusion coefficients are zero in the vicinity of equatorial pitch angle $\alpha = 90°$ [cf. *Summers et al.*, 2007; *Albert*, 2008; *Ukhorskiy et al.*, 2010], and so EMIC waves are theoretically not capable of isotropizing a distribution function away from that 90° vicinity. Evolution toward isotropy is seen in the observations of the radiation belt electrons. It may be possible that for finite-amplitude EMIC waves, the quasilinear description may be lacking and $D_{\alpha\alpha}$ might be nonzero near 90°; test particle simulations (for ions) indicate that this might be the case [cf. *de Soria-Santacruz et al.*, 2013]. It may also be possible that magnetosonic waves act to move the radiation electrons away from 90° in the plumes; for magnetosonic waves the nonzero $D_{\alpha\alpha}$ coefficient extends close to 90° for high values of ω_{pe}/ω_{ce}

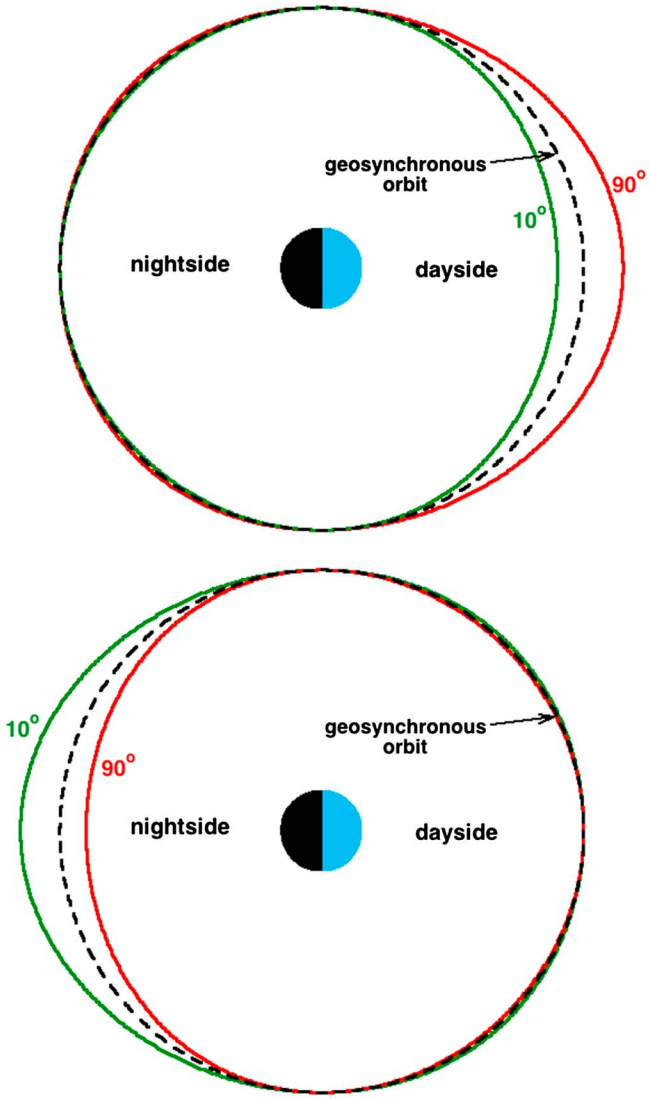

Figure 7. With the Sun to the right, geosynchronous orbit in the equatorial magnetosphere is shown as the dashed black circle. (top) The drift shell splitting of electrons colocated on the nightside is depicted, and (bottom) the drift shell splitting of electrons colocated on the dayside is depicted.

such as those that occur in plumes [cf. *Horne et al*., 2007; *Mourenas et al*., 2013]. The combination of EMIC waves and magnetosonic waves may be able to explain the observed evolution toward isotropy of the 1.5 MeV electrons. Future studies of the scattering in plumes using SOPA measurements with higher-pitch angle resolution and with higher-energy resolution may resolve this 90° dilemma and may shed light on the type of plasma waves giving rise to the scattering.

In estimating $D_{\alpha\alpha}$ for the plume plasma it was assumed that there is electron scattering throughout the plume. But the distribution of plasma waves may not be uniform within the plumes. For example, in *Summers et al*. [2007, Figure 21] EMIC waves are depicted being concentrated on the duskward edge of a plume where fresh plasma sheet ions drift into the plume plasma; perhaps this is motivated by the concept that the free energy of the hot ions becomes depleted in the plume plasma, and the waves can only be driven on the duskward edge. It remains to be determined what the distribution of EMIC waves is within plumes. If the EMIC waves do the scattering and if the EMIC waves are concentrated on the plume edge, then the pitch angle scattering rates calculated from the observations in this paper are underestimates for the rates while the electrons are within the active wave regions.

Owing to the existence of a minimum kinetic energy for electrons to cyclotron resonate with EMIC waves [cf. *Meredith et al*., 2003; *Ukhorskiy et al*., 2010], EMIC waves cannot be producing the observed radiation belt pitch angle scattering in the 120–180 keV band. However, the $D_{\alpha\alpha}$ value of 2.4×10^{-4} rad^2 s^{-1} obtained for 150 keV electrons is in the ballpark of the *Summers et al*. [2008] theoretical estimates of the pitch angle diffusion coefficients for plasmaspheric hiss inside of plasmaspheric drainage plumes shown in *Summers et al*. [2008, Figure 2].

7. Radial Transport Produced by the Pitch Angle Scattering

In Figure 7 (top) a group of electrons starting out colocated at geosynchronous orbit on the nightside is shown orbiting to the dayside. An electron with a 90° pitch angle (red curve) orbits out further from the Earth on the dayside then does an electron with a near-parallel pitch angle of 10° (green curve). In Figure 7 (bottom) a group of electrons starting out colocated at geosynchronous orbit on the dayside is shown orbiting into the nightside; in this case the 90° electrons (red curve) orbit closer to the Earth on the nightside then do the electrons with 10° pitch angles (green curve). At geosynchronous orbit the radial profile of the electron radiation belt is such that the electron fluxes are higher closer to the Earth. With that radial profile in mind,

Table 3. Estimating the Magnitude of the Radial Diffusion Coefficient D_{rr} at Geosynchronous Orbit Associated With Pitch Angle Scattering Inside of the Drainage Plume, Based on a Radial Displacement of ~ 0.5 R_E Associated With Shell Splitting

	1.3–1.7 MeV	120–180 keV
Δr	0.5 R_E	0.5 R_E
τ_{isot}	1800 s	5600 s
$D_{rr} = (\Delta r)^2/\tau_{isot}$	5600 $km^2\ s^{-1}$	1800 $km^2\ s^{-1}$
D_{LL}	12 day^{-1}	3.8 day^{-1}

Figure 7 (bottom) can be interpreted as follows. The electrons that are observed in geosynchronous orbit on the dayside originated from different radial distances on the nightside: the 90° electrons on the dayside came from deeper in the magnetosphere on the nightside where the fluxes are higher and the parallel electrons on the dayside came from larger radial distances on the nightside where the fluxes are weaker. Hence, at geosynchronous orbit on the dayside the perpendicular fluxes dominate the parallel fluxes and the anisotropy of the radiation belt is perpendicular dominated. Similarly, Figure 7 (top) can be interpreted to explain the parallel-dominated anisotropy of the electron radiation belt at geosynchronous orbit on the night side.

Pitch angle scattering in the presence of drift shell splitting will produce radial diffusion [*Falthammar and Walt*, 1969; *Roederer and Schulz*, 1969]. Changing the pitch angle of an electron on one side of the Earth changes the spatial location of its orbit on the other side of the Earth. For a population of colocated electrons in the dayside magnetosphere, the electrons that have more-parallel pitch angles will orbit farther from the Earth on the nightside than those electrons that have more-perpendicular pitch angles (cf. Figure 7 (bottom)); hence, the pitch angle scattering in the plume on the dayside (where the electron distribution is perpendicular dominated) will produce a net movement of pitch angles from perpendicular to parallel and as a result will produce a net radial transport of radiation belt electrons outward in the nightside magnetosphere. Likewise if there is pitch angle scattering on the nightside where the distribution is parallel dominated, the scattering will produce a net transfer from parallel pitch angles to perpendicular pitch angles, and that nightside pitch angle diffusion will produce a net outward radial transport of radiation belt electrons on the dayside (cf. Figure 7 (top)).

In Table 3 estimates of the order of magnitude of the radial-diffusion coefficients for radiation belt electrons associated with the pitch angle scattering of the electrons in the plasmaspheric drainage plume are made. Drift shell splitting at geosynchronous orbit results in radial displacements of the electron orbits on the order of 0.5 R_E [cf. *Selesnick and Blake*, 2002, Figure 3] (with the size of those shell-splitting radial displacements depending on the state of the magnetosphere). Hence, when scattering the pitch angles of the electrons, spatial displacements of Δr on the order of 0.5 R_E result. This value for Δr is entered into Table 3. The time step associated with this radial step is τ_{isot}. Constructing a radial-diffusion coefficient D_{rr} as

$$D_{rr} \sim (\Delta r)^2/\tau_{isot}, \tag{6}$$

for 1.3–1.7 MeV electrons with $\tau_{isot} = 1800$ s (see Table 1) and $\Delta r = 0.5\ R_E$, expression (6) yields $D_{rr} \sim 5600\ km^2\ s^{-1}$ which is $D_{LL} \sim 12\ day^{-1}$; for 120–180 keV electrons with $\tau_{isot} = 5600$ s (see Table 1) and $\Delta r = 0.5\ R_E$ expression (6) yields $D_{rr} \sim 1800\ km^2\ s^{-1}$ which is $D_{LL} \sim 3.8\ day^{-1}$. These values for the radiation belt electrons at geosynchronous orbit are entered into Table 3.

Note that these D_{rr} and D_{LL} values in Table 3 associated with plume pitch angle scattering are upper limits: pitch angle scattering in the nightside magnetosphere must occur to fully utilize the dayside pitch angle scattering to produce true radial diffusion.

The radial-diffusion coefficients estimated here for pitch angle scattering of radiation belt electrons in the drainage plume are of the order of the radial-diffusion coefficients commonly calculated for radiation belt electron interactions with magnetospheric ULF waves. For examples, the $D_{LL} = 12\ day^{-1}$ value in Table 3 for 1.5 MeV equals the *Brautigam and Albert* [2000] radial-diffusion coefficient formula $D_{LL}(Kp) = L^{10}\ 10^{(0.506\,Kp\,-\,9.325)}$ for $Kp = 4.37$ and the $D_{LL} = 3.8\ day^{-1}$ value in Table 3 for 150 keV equals the *Brautigam and Albert* [2000] radial-diffusion coefficient formula for $Kp = 3.38$; the Table 3 D_{LL} values at geosynchronous orbit are in the range of values of *Shprits et al.* [2008, Figure 5]; the $D_{LL} = 12\ day^{-1}$ value in Table 3 for 1.5 MeV is in close agreement with the formula $D_{LL} = (1.5 \times 10^{-6}\ day^{-1})L^{8.5}$ of *Fei et al.* [2006]; the $D_{LL} = 12\ day^{-1}$ value in Table 3 for 1.5 MeV is somewhat higher than the 1 MeV and 2 MeV values for geosynchronous orbit during a mild storm in *Tu et al.* [2012, Figure 8a]; and the $D_{LL} = 12\ day^{-1}$ value in Table 3 for 1.5 MeV is approximately equal to the 1 MeV $Kp = 6$ "mapped" D_{LL} value in *Ozeke et al.* [2012, Figure 11].

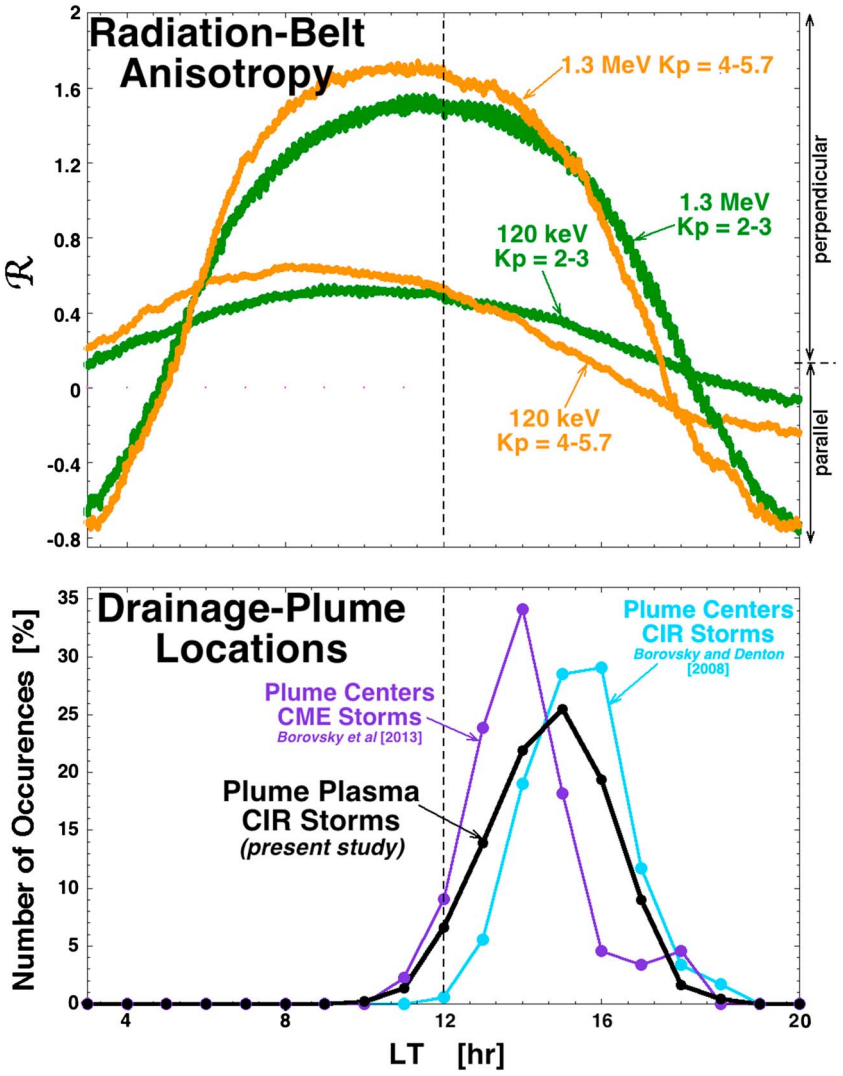

Figure 8. (top) The local time trend of the pitch angle anisotropy ratio at in geosynchronous orbit is plotted as a function of local time across the dayside magnetosphere. The green curves are 500-point running averages of 157,840 10 min averaged values of *R* that were measured when the *Kp* index was $2 \le Kp \le 3$, and the orange curves are 500-point running averages of 56,476 10 min averaged values of *R* that were measured when the *Kp* index was $4 \le Kp \le 5.7$. (bottom) The occurrence distribution of plasmaspheric drainage plumes at geosynchronous orbit is plotted from three sources (see text). In both panels local noon is marked with the vertical dashed line.

8. Discussion

Substantial amounts of pitch angle scattering were statistically detected as radiation belt electrons drift across the plasmaspheric drainage plume in the dayside magnetosphere. At geosynchronous orbit the anisotropy of the radiation belt electron population is reduced in a single crossing of the plume by about 25% at 1.3–1.7 MeV and by about 55% at 120–180 keV.

This pitch angle scattering of the radiation belt electrons as they traverse the plume results in an offset of the anisotropy profile across the dayside magnetosphere at high *Kp* when plumes are present. This can be seen Figure 8 (top) where all available anisotropy measurements from six geosynchronous spacecraft in the years 1999–2007 are displayed. Five hundred-point running averages of the measured anisotropy ratio *R* are plotted as functions of local time for all data taken when the *Kp* index was between $2 \le Kp \le 3$ (green curves) and between $4 \le Kp \le 5.7$ (orange curves). The upper curves are for 1.3–1.7 MeV electrons, and the lower curves are for 120–180 keV electrons. As can be seen for both energy bands, the green curves at lower *Kp* (where plumes are not likely to be present in the dayside magnetosphere) are approximately symmetric

across local noon with the anisotropy maximized approximately at noon. However, for both energy bands the orange curves at higher *Kp* (where plasmaspheric drainage plumes are persistently seen in the afternoon magnetosphere) are very asymmetric across noon, with stronger anisotropies in the morning sector then in the afternoon sector. In Figure 8 (bottom) the statistical locations of plasmaspheric drainage plumes are plotted as functions of local time. The black curve is a binning of the local times at which drainage plume plasma was located by the MPA instruments in the present study of 226 plume crossings during high-speed stream-driven storms (corotating interaction region (CIR) storms); the light blue curve is a binning of the center positions of the drainage plumes collected in the *Borovsky and Denton* [2008] survey of drainage plumes during CIR-driven storms and the purple curve in Figure 8 (bottom) is a binning of the center positions of the drainage plumes collected in the *Borovsky et al.* [2013] survey of drainage plumes during coronal mass ejection-driven storms. The across-noon asymmetry in the higher-*Kp* radiation belt anisotropy ratios in the Figure 8 (top) is consistent with a strong reduction in the anisotropy as the radiation belt electrons drift from the morningside into the drainage plumes in the afternoon sector.

The pitch angle scattering of radiation belt electrons has consequences besides an evolution toward isotropy. One consequence is the scattering of radiation belt electrons into the atmospheric loss cone and a decay of the radiation belt [e.g., *Millan and Thorne*, 2007; *Meredith et al.*, 2011]. The temporal rate of decay depends not only on the scattering rate but also on the detailed profile of the pitch angle diffusion coefficient in the vicinity of the loss cone [cf. *Glauert and Horne*, 2005; *Shprits et al.*, 2009].

A second consequence of the pitch angle scattering of radiation belt electrons is that it acts as a catalyst enabling magnetic pumping [cf. *Alfven and Falthammar*, 1963] of the radiation belt electrons. In magnetic pumping an interplay between compressible ULF waves and pitch angle scattering makes the plasma compressions and decompressions by the ULF waves irreversible, resulting in a net energy transfer from the ULF waves to the radiation belt electrons [*Borovsky*, 1986; *Liu et al.*, 1999].

A third consequence of pitch angle scattering in the presence of drift shell splitting is that it produces radial diffusion, as discussed in section 7.

Acknowledgments

The authors wish to thank Mike Henderson for helpful conversations and to thank Rod Christensen for data. This work was supported at the University of Michigan by the NASA Geospace SR&T Program; at the Space Science Institute by the NSF GEM Program, the NASA CCMSC-24 Program, and the NASA Heliophysics Guest Investigators Program; and at the University of Lancaster by Science and Technology Funding Council grant ST/I000801/1. The geosynchronous data were provided by the USNDS Program funded by the U.S. Department of Energy.

Philippa Browning thanks the reviewers for their assistance in evaluating this paper.

References

Albert, J. M. (2008), Efficient approximations of quasi-linear diffusion coefficients in the radiation belts, *J. Geophys. Res.*, *113*, A06208, doi:10.1029/2007JA012936.

Alfven, H., and C.-G. Falthammar (1963), *Cosmical Electrodynamics*, Sect. 2.7.4, Oxford Univ. Press, New York.

Artemyev, A., O. Agapitov, V. Krasnoselskikh, H. Breuillard, and G. Rolland (2012), Statistical model of electron pitch angle diffusion in the outer radiation belt, *J. Geophys. Res.*, *117*, A08219, doi:10.1029/2012JA017826.

Bame, S. J., D. J. McComas, M. F. Thomsen, B. L. Barraclough, R. C. Elphic, J. P. Glore, J. T. Gosling, J. C. Chavez, E. P. Evans, and F. J. Wymer (1993), Magnetospheric plasma analyzer for spacecraft with constrained resources, *Rev. Sci. Instrum.*, *64*, 1026.

Belian, R. D., G. R. Gisler, T. Cayton, and R. Christensen (1992), High-Z energetic particles at geosynchronous orbit during the great solar proton event series of October 1989, *J. Geophys. Res.*, *97*, 16,897–16,906.

Borovsky, J. E. (1986), Magnetic pumping by magnetosonic waves in the presence of non-compressive electromagnetic fluctuations, *Phys. Fluids*, *29*, 3245.

Borovsky, J. E., and M. H. Denton (2006), The differences between CME-driven storms and CIR-driven storms, *J. Geophys. Res.*, *111*, A07S08, doi:10.1029/2005JA011447.

Borovsky, J. E., and M. H. Denton (2008), A statistical look at plasmaspheric drainage plumes, *J. Geophys. Res.*, *113*, A09221, doi:10.1029/2007JA012994.

Borovsky, J. E., and M. H. Denton (2010a), The magnetic field at geosynchronous orbit during high-speed-stream-driven storms: Connections to the solar wind, the plasma sheet, and the outer electron radiation belt, *J. Geophys. Res.*, *115*, A08217, doi:10.1029/2009JA015116.

Borovsky, J. E., and M. H. Denton (2010b), On the heating of the outer radiation belt to produce high fluxes of relativistic electrons: Measured heating rates for high-speed-stream-driven storms, *J. Geophys. Res.*, *115*, A12206, doi:10.1029/2010JA015342.

Borovsky, J. E., and M. H. Denton (2011), A survey of the anisotropy of the outer electron radiation belt during high-speed-stream-driven storms, *J. Geophys. Res.*, *116*, A05201, doi:10.1029/2010JA016151.

Borovsky, J. E., B. Lavraud, and M. M. Kuznetsova (2009), Polar cap potential saturation, dayside reconnection, and changes to the magnetosphere, *J. Geophys. Res.*, *114*, A03224, doi:10.1029/2009JA014058.

Borovsky, J. E., M. H. Denton, R. E. Denton, V. K. Jordanova, and J. Krall (2013), Estimating the effects of ionospheric plasma on solar-wind/magnetosphere coupling via mass loading of dayside reconnection: Ion-plasma-sheet oxygen, plasmaspheric drainage plumes, and the plasma cloak, *J. Geophys. Res. Space Physics*, *118*, 5695–5719, doi:10.1002/jgra.50527.

Bortnik, J., R. M. Thorne, T. P. O'Brien, J. C. Green, R. J. Strangeway, Y. Y. Shprits, and D. N. Baker (2006), Observation of two distinct, rapid loss mechanisms during the 20 November 2003 radiation belt dropout event, *J. Geophys. Res.*, *111*, A12216, doi:10.1029/2006JA011802.

Brautigam, D. H., and J. M. Albert (2000), Radial diffusion analysis of outer radiation belt electrons during the October 9, 1990 magnetic storm, *J. Geophys. Res.*, *105*, 291–309.

Cayton, T. E., and R. D. Belian (2007), Numerical modeling of the synchronous orbit particle analyzer (SOPA, version 2) that flew on S/C 1990–095, LA Rep. LA-14335, Los Alamos Natl. Lab., Los Alamos, NM 87545.

Chan, K.-W., and R. E. Holzer (1976), ELF hiss associated with plasma density enhancements in the outer magnetosphere, *J. Geophys. Res.*, *81*, 2267–2274.

Chanteur, G., R. Gendrin, and S. Perraut (1978), High-energy electron drift echoes at the geostationary orbit, *J. Atmos. Terr. Phys.*, *40*, 367–371.
Chappell, C. R., M. M. Huddleston, T. E. Moore, B. L. Giles, and D. C. Delcourt (2008), Observations of the warm plasma cloak and an explanation of its formation in the magnetosphere, *J. Geophys. Res.*, *113*, A09206, doi:10.1029/2007JA012945.
Denton, M. H., and J. E. Borovsky (2008), Superposed epoch analysis of high-speed-stream effects at geosynchronous orbit: Hot plasma, cold plasma, and the solar wind, *J. Geophys. Res.*, *113*, A07216, doi:10.1029/2007JA012998.
Denton, M. H., and J. E. Borovsky (2012), Magnetosphere response to high-speed solar wind streams: A comparison of weak and strong driving and the importance of extended periods of fast solar wind, *J. Geophys. Res.*, *117*, A00L05, doi:10.1029/2011JA017124.
de Soria-Santacruz, M., K. G. Orlova, M. Martinez-Sanchez, and Y. Y. Shprits (2013), Scattering rates of inner belt protons by EMIC waves: A comparison between test particle and diffusion simulations, *Geophys. Res. Lett.*, *40*, 4793–4797, doi:10.1002/grl.50925.
Falthammar, C.-G., and M. Walt (1969), Radial motion resulting from pitch-angle scattering of trapped electrons in the distorted geomagnetic field, *J. Geophys. Res.*, *74*, 4184–4186.
Fei, Y., A. A. Chan, S. R. Elkington, and M. J. Wiltberger (2006), Radial diffusion and MHD particle simulations of relativistic electron transport by ULF waves in the September 1998 storm, *J. Geophys. Res.*, *111*, A12209, doi:10.1029/2005JA011211.
Fraser, B. J., T. M. Loto'aniu, and H. J. Singer (2006), Electromagnetic ion cyclotron waves in the magnetosphere, in *Magnetospheric ULF Waves*, edited by K. Takahashi et al., pp. 195–212, AGU, Washington, D. C.
Friedel, R. H. W., G. D. Reeves, and T. Obara (2002), Relativistic electron dynamics in the inner magnetosphere—A review, *J. Atmos. Sol. Terr. Phys.*, *64*, 265.
Gannon, J. L., X. Li, and D. Heynderickx (2007), Pitch angle distribution analysis of radiation belt electrons based on Combined Release and Radiation Effects Satellite Medium Electrons A data, *J. Geophys. Res.*, *112*, A05212, doi:10.1029/2005JA011565.
Glauert, S. A., and R. B. Horne (2005), Calculation of pitch angle and energy diffusion coefficients with the PADIE code, *J. Geophys. Res.*, *110*, A04206, doi:10.1029/2004JA010851.
Hayakawa, M., N. Ohmi, M. Parrot, and F. Lefeuvre (1986), Direction finding of ELF hiss emissions in a detached plasma region of the magnetosphere, *J. Geophys. Res.*, *91*, 135–141.
Hones, E. W. (1963), Motions of charged particles trapped in the Earth's magnetosphere, *J. Geophys. Res.*, *68*, 1209–1219.
Horne, R. B., R. M. Thorne, S. A. Glauert, N. P. Meredith, D. Pokhotelov, and O. Santolik (2007), Electron acceleration in the Van Allen radiation belts by fast magnetosonic waves, *Geophys. Res. Lett.*, *34*, L17107, doi:10.1029/2007GL030267.
Jordanova, V. K., Y. S. Miyoshi, S. Zaharia, M. F. Thomsen, G. D. Reeves, D. S. Evans, C. G. Mouikis, and J. F. Fennell (2006), Kinetic simulations of ring current evolution during the Geospace Environment Modeling challenge events, *J. Geophys. Res.*, *111*, A11S10, doi:10.1029/2006JA011644.
Jordanova, V. K., M. Spasojevic, and M. F. Thomsen (2007), Modeling the electromagnetic ion cyclotron wave-induced formation of detached supauroral proton arcs, *J. Geophys. Res.*, *112*, A08209, doi:10.1029/2006JA012215.
Jordanova, V. K., J. Albert, and Y. Miyoshi (2008), Relativistic electron precipitation by EMIC waves from self-consistent global simulations, *J. Geophys. Res.*, *113*, A00A10, doi:10.1029/2008JA013239.
Kovalevskiy, I. V. (1980), Ion-cyclotron instability in the frontal boundary layer of the geomagnetosphere produced by detached plasma clouds, *Geomagn. Aeron.*, *20*, 338–341.
Kovalevskiy, I. V. (1981), Cyclotron instability during interaction of detached plasma regions with the plasma sheet during substorms, *Geomagn. Aeron.*, *21*, 83.
Lam, M. M., R. B. Horne, N. P. Meredith, and S. A. Glauert (2009), Radiation belt electron flux variability during three CIR-driven geomagnetic storms, *J. Atmos. Sol. Terr. Phys.*, *71*, 1145–1156.
Liu, W. W., G. Rostoker, and D. N. Baker (1999), Internal acceleration of relativistic electrons by large-amplitude ULF pulsations, *J. Geophys. Res.*, *104*, 17,391–17,407.
Lyons, L. R., and R. M. Thorne (1973), Equilibrium structure of radiation belt electrons, *J. Geophys. Res.*, *78*, 2142–2149.
McPherron, R. L., D. N. Baker, and N. U. Crooker (2009), Role of the Russell-McPherron effect in the acceleration of relativistic electrons, *J. Atmos. Sol. Terr. Phys.*, *71*, 1032–1044.
Meredith, N. P., R. M. Horne, R. B. Horne, D. Summers, B. J. Fraser, and R. R. Anderson (2003), Statistical analysis of relativistic electron energies for cyclotron resonance with EMIC waves observed on CRRES, *J. Geophys. Res.*, *108*(A6), 1250, doi:10.1029/2002JA009700.
Meredith, N. P., R. B. Horne, M. M. Lam, M. H. Denton, J. E. Borovsky, and J. C. Green (2011), Energetic electron precipitation during high-speed solar wind stream driven storms, *J. Geophys. Res.*, *116*, A05223, doi:10.1029/2010JA016293.
Millan, R. M., and R. M. Thorne (2007), Review of radiation belt relativistic electron losses, *J. Atmos. Sol. Terr. Phys.*, *69*, 362–377.
Mourenas, D., A. V. Artemyev, O. V. Agaapitov, and V. Krasnoelskikh (2013), Analytical estimates of electron quasi-linear diffusion by fast magnetosonic waves, *J. Geophys. Res. Space Physics*, *118*, 3096–3112, doi:10.1002/jgra.50349.
Ozeke, L. G., I. R. Mann, K. R. Murphy, I. J. Rae, D. K. Milling, S. R. Elkington, A. A. Chan, and H. J. Singer (2012), ULF wave derived radiation belt radial diffusion coefficients, *J. Geophys. Res.*, *117*, A04222, doi:10.1029/2011JA017463.
Paulikas, G. A., and J. B. Blake (1976), Modulation of trapped energetic electrons at 6.6 Re by the interplanetary magnetic field, *Geophys. Res. Lett.*, *3*, 277–280.
Pfitzer, K. A., T. W. Lezniak, and J. R. Winckler (1969), Experimental verification of drift-shell splitting in the distorted magnetosphere, *J. Geophys. Res.*, *74*, 4687–4693.
Roederer, J. G., and M. Schulz (1969), Effect of shell splitting on radial diffusion in the magnetosphere, *J. Geophys. Res.*, *74*, 4117–4122.
Selesnick, R. S., and J. B. Blake (2002), Relativistic electron drift shell splitting, *J. Geophys. Res.*, *107*(A9), 1265, doi:10.1029/2001JA009179.
Shprits, Y. Y., S. R. Elkington, N. P. Meredith, and D. A. Subbotin (2008), Review of modeling of losses and sources of relativistic electrons in the outer radiation belt I: Radial transport, *J. Atmos. Sol. Terr. Phys.*, *70*, 1679–1693.
Shprits, Y. Y., L. Chen, and R. M. Thorne (2009), Simulations of pitch angle scattering of relativistic electrons with MLT-dependent diffusion coefficients, *J. Geophys. Res.*, *114*, A03219, doi:10.1029/2008JA013695.
Spasojevic, M., and S. A. Fuselier (2009), Temporal evolution of proton precipitation associated with the plasmaspheric plume, *J. Geophys. Res.*, *114*, A12201, doi:10.1029/2009JA014530.
Spasojevic, M., H. U. Frey, M. F. Thomsen, S. A. Fuselier, S. P. Gary, B. R. Sandel, and U. S. Inan (2004), The link between a detached subauroral proton arc and a plasmaspheric plume, *Geophys. Res. Lett.*, *31*, L04803, doi:10.1029/2003GL018389.
Summers, D., B. Ni, and N. Meredith (2007), Timescales for radiation belt electron acceleration and loss due to resonant wave-particle interactions: 2. Evaluation for VLF chorus, ELF hiss, and electromagnetic ion cyclotron waves, *J. Geophys. Res.*, *112*, A04207, doi:10.1029/2006JA011993.
Summers, D., B. Ni, N. P. Meredith, R. B. Horne, R. M. Thorne, M. B. Moldwin, and R. R. Anderson (2008), Electron scattering by whistler-mode ELF hiss in plasmaspheric plumes, *J. Geophys. Res.*, *113*, A04219, doi:10.1029/2007JA012678.
Thomsen, M. F., E. Noveroske, J. E. Borovsky, and D. J. McComas (1999), Calculating the moments from measurements by the Los Alamos magnetospheric plasma analyzer, LA-13566-MS, Los Alamos National Laboratory.

Thorne, R. M., R. B. Horne, V. K. Jordanova, J. Bortnik, and S. Glauert (2006), Interaction of EMIC waves with thermal plasma and radiation belt particles, in *Magnetospheric ULF Waves*, edited by K. Takahashi et al., pp. 213–223, AGU, Washington, D. C.

Tu, W., S. R. Elkington, X. Li, W. Liu, and J. Bonnell (2012), Quantifying radial diffusion coefficients of radiation belt electrons based on global MHD simulation and spacecraft measurements, *J. Geophys. Res.*, *117*, A10210, doi:10.1029/2012JA017901.

Ukhorskiy, A. Y., Y. Y. Shprits, B. J. Anderson, K. Takahashi, and R. M. Thorne (2010), Rapid scattering of radiation belt electrons by storm-time EMIC waves, *Geophys. Res. Lett.*, *37*, L09101, doi:10.1029/2010GL042906.

West, H. I., R. M. Buck, and J. R. Walton (1973), Electron pitch angle distributions throughout the magnetosphere as observed on Ogo 5, *J. Geophys. Res.*, *78*, 1064–1081.

Yahnin, A. G., and T. A. Yahnina (2007), Energetic proton precipitation related to ion-cyclotron waves, *J. Atmos. Sol. Terr. Phys.*, *69*, 1690–1706.